

# EXPERIMENTAL AND NUMERICAL ANALYSIS OF DEFORMATION PATTERNS IN NOTCHED HETEROGENEOUS WELDS

Marc Giménez Avalos<sup>1</sup>, Florence Keppens<sup>1</sup>, Sameera Naib<sup>2</sup>, Wim De Waele<sup>2</sup>, Stijn Hertelé<sup>2</sup>

<sup>1</sup> Ghent University, Belgium

<sup>2</sup> Ghent University, Soete Laboratory, Belgium

**Abstract:** Standardized weld flaw assessment techniques assume the weld region to be homogeneous which is a strong idealisation of reality. Characterising the effects of heterogeneous properties of welds through the analysis of deformation patterns and slip lines is the major concern of this research. It is the goal to investigate which effects these variations in properties within the weld material have on the propagation of cracks within the weld material. Performed experiments are SENT tests on strongly heterogeneous welded connections. The same material is also simulated with a weld heterogenisation model in ABAQUS®. Results from both experiments and simulations are discussed and compared. It is shown that slip lines tend to avoid zones of high hardness in a way that a path of least resistance is found. Related to this, it is seen that the slip line angles deviate from the theoretical 45° for homogeneous material. Obtained results validate the numerical model used.

**Keywords:** ECA, weld heterogeneity, SENT, deformation behaviour, slip line

## 1 INTRODUCTION

Welded steel connections are widely used in many applications such as pipelines and offshore structures. However, welds inevitably contain flaws and are heterogeneous in terms of constitutive behaviour. In terms of safety and from an economical point of view, the structural integrity of welds containing defects is of high importance. Defects rejected by workmanship rules are analysed by means of a fracture mechanics based analysis, referred to as Engineering Critical Assessment (ECA). Over the years, these standards evolved by considering the strength mismatch between the base material, weld material and heat affected zones (HAZ) [1, 2]. Nonetheless, all ECA standards assume the weld to be homogeneous, necessitating conservative assumptions [3]. To account for heterogeneity within a weld ECA, the authors are performing research in characterising the effect of heterogeneity on the deformation behaviour of notched welded connections. The authors are developing techniques to account for constitutive heterogeneity within weld ECA. A promising approach is to assume homogeneous welds having average properties along patterns of strain concentration originating from the crack tip. Under tension loading, slip line theory predicts these patterns to be linear and oriented at 45° with respect to the load direction for homogeneous materials. The soundness of this prediction is questionable in presence of constitutive heterogeneity. Therefore, in this paper, experimental and numerical analysis of deformation patterns within tension loaded welds containing defects will be analysed, with the objective to evaluate the soundness of predictions based on slip line theory in presence of heterogeneity. Details on the used materials and experimental and numerical simulations methods are given in Section 2. Results are represented and discussed in Section 3.

## 2 MATERIALS AND METHODS

### 2.1 Material

The specimens tested are extracted from welded plates (400x500x25 mm<sup>3</sup>) provided by the University of Maribor. The welding process is metal active gas welding (MAG). The base material is hot rolled structural steel S690QT. Two different filler materials are used in the making of the specimens. Purposely, the weld is created in such a way that one side of the X-shaped weld configuration is an overmatching zone (stronger properties than the base material: MIG90 (EN ISO 16834-A: G89 6 M Mn4Ni2CrMo)) and the other side of the weld is undermatching (weaker properties than base material: VAC65 (EN ISO 14341-A: G46A 4 M2/M3/C1 4 Si1)). The intended levels of over- and undermatch are 30%. The goal is the investigation of deformations in the vicinity of the crack and how these can be related to crack driving force. To represent a crack in the weld material, a notch is applied in the centre of the weld. Side grooves are machined, resulting in a width reduction of 7.5% on both sides, to promote uniform crack extension.

## 2.2 Experimental Techniques

### 2.2.1 Hardness mapping

To characterise and quantify heterogeneity of welds, specimens are extracted from different places in the welded connection and hardness is mapped. Using approximately 1400 indents on the small surface shown on Figure 1, the hardness across the entire weld cross section is measured. From the obtained hardness values, a contour plot is made to visualise and to quantify the variation in material properties. The Vickers hardness map is produced with 5 kgf indent load (HV5) following ASTM E384-11 [4].

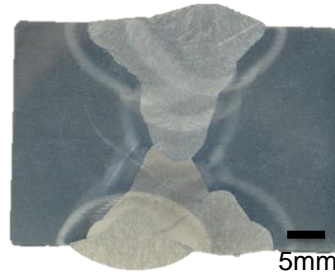


Figure 1: Macrograph of the weld

### 2.2.2 SENT testing

Thin-walled tubular structures (such as pipelines) are generally loaded in tension due to their low thickness to diameter ratio. SENB and CT specimens are too conservative for this application due to the imposed bending moment herein. Low-constraint fracture toughness tests such as the Single Edge Notched Tension (SENT) test serve as an alternative with reduced conservatism [5, 6, 7]. The experiments performed in this research are SENT tests on welded connections in which a defect is represented as a notch in the weld material centre. The specimens were hydraulically clamped within a 1000kN test bench. One side of the specimen is clamped in fixed position, while the other side is displacement controlled at 0.002 mm/s. Initial notch depth is set to  $\frac{a_0}{W} = 0.3$  and side grooves result in a total width reduction of 15% and have a tip radius of 40 $\mu$ m. During testing, synchronised measurements are performed to obtain information about the load, crack driving force, crack extension and deformation behaviour of the specimen.

Crack driving force is represented by means of crack tip opening displacement (CTOD) [8, 9, 6]. Quantification of CTOD is performed by the usage of two clip gauges, mounted over the notch at different heights using the procedure described by BS8571:214 [10].

The deformation behaviour of the specimen during the test is monitored using 3D digital image correlation (3D DIC). On one side of the specimen, a black speckle pattern is painted on a white primer. Devoted postprocessing allows for the localisation and investigation of the paths of maximum equivalent strain, further referred to as: slip lines.

Ductile crack extension is measured during SENT tests using the Direct Current Potential Drop (DCPD) method using a DC power supply. A constant DC current of about 50 A is hereby forced through the specimen at a potential between the current pins of approximately 0.70 V. The crack depth in the specimen is related to the drop in voltage over the crack, as electric resistance increases when the crack ligament becomes smaller. Important during the measurement of potential drop is the presence of a reference potential drop measurement at a location between the current pins, but at a distance from the crack. Normalisation against this reference signal allows to compensate for effects of current leaks, temperature changes (e.g. by the Joule effect) and noise caused by the power supply.

The experimental test matrix at hand is presented in Table 1. In total, four SENT specimens are tested: two where the initial notch is located within the OM region of the weld, having the crack propagate towards the UM region and two where the initial notch is located within the UM region of the weld, having the crack propagate towards the OM region. The geometry of the specimens is the same for all specimens to ensure proper results to compare the results with simulated ones.

Table 1: Test matrix

| Specimen name | Notch location | Width W (mm) | Thickness B (mm) | Daylight length L (mm) | Notch depth $a_0/W$ | Side grooves |
|---------------|----------------|--------------|------------------|------------------------|---------------------|--------------|
| OM-1, OM-2    | OM             | 20           | 20               | 200                    | 0.3                 | yes          |
| UM-1, UM-2    | UM             | 20           | 20               | 200                    | 0.3                 | yes          |

## 2.3 Numerical Techniques

### 2.3.1 Finite element model

The effects of heterogeneity of the weld are also investigated by means of simulations with a 3D finite element model in ABAQUS® version 6.11. The model has been developed by Verstraete et al. [11, 12] and is generated by an in-house parametric Python™ script, which allows for the systematic generation, meshing and analysis of a multitude of models with different geometrical and/or material properties. The geometry and clamping specification adopted follow the experimental procedure for SENT testing [13, 11]. In agreement with the experiments, one end of the specimen is clamped, whereas the other end is moved under displacement control. The specimen has a daylight length  $L=10W$  and equal width  $W$  and thickness  $B$ . The side grooves have each a relative depth of 7.5%, an opening angle of  $90^\circ$  and a root radius of 0.4 mm. An important parameter is the relative crack depth  $a_0/W$  of the notch, which equals 0.3 in line with the experiments. The tip of the initially blunted notch has a radius of  $75\mu\text{m}$ . Eight noded brick elements with reduced integration (ABAQUS® type C3D8R) are used. In this investigation, the simulations contain around 25000 elements. The density of the meshing increases towards the crack tip, where a fine spider web grid is implemented. As large deformations are present, the model considers non-linear geometrical effects (e.g. collapse phenomena) for strain calculations and isotropic  $J_2$  plasticity is introduced [12, 11]. Illustration of the used model is given in Figure 2.

Material properties obtained from the hardness maps are assigned to each element as explained in the paper of Hertelé et al. [11]. Different standard transfer functions that convert hardness values into constitutive (stress-strain) properties have been investigated in [14]. In this paper, the following procedure is adopted. Stress-strain behaviour is represented by the Ramberg-Osgood equation, i.e.:

$$\frac{\epsilon}{\epsilon_y} = \frac{\sigma}{\sigma_y} + \alpha \left( \frac{\sigma}{\sigma_y} \right)^n \quad (2)$$

In this equation,  $\sigma_y$  and  $\epsilon_y = \sigma_y/E$  are yield strength and yield strain respectively (related through Young's modulus  $E$ ).  $\alpha$  is the yield offset parameter which is set to  $0.002/\epsilon_y$  so that  $\sigma_y$  represents the 0.2% proof stress.  $n$  is the strain hardening exponent, closely related to the yield to tensile ratio  $Y/T$  according to Considère's necking criterion, by means of the following curve-fitted expression:  $n=2.4+2.9(Y/T)/(1-0.95(Y/T))$ . Hereby,  $Y/T$  is calculated as  $1/[1.07 + (\frac{350}{R_m})^{2.5}]$  where  $R_m$  equals  $3.0HV + 22.1$ .

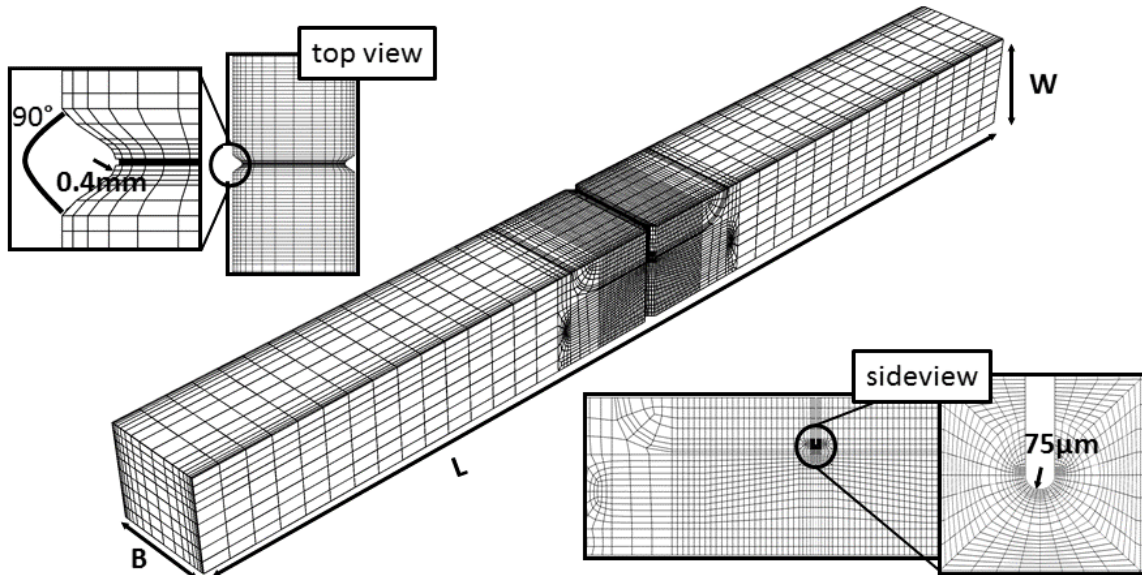


Figure 2: SENT model as modelled in ABAQUS®

### 2.3.2 Slip line analysis

An algorithm has been previously developed by Filip Van Gerven (in MatLab®) to locate the lines of maximum strain originating from the notch tip of a SENT specimen [15]. These lines are further referred to as slip lines. The algorithm can be used to define the slip lines from data obtained from both SENT simulations and experiments analysed with digital image correlation (DIC). In this model, the slip lines are

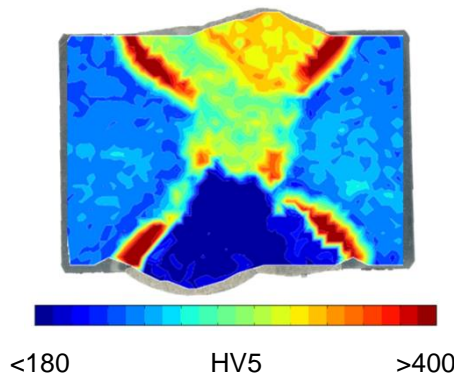
defined as the path of maximum equivalent plastic strain for simulations, and maximum equivalent total strain for experiments. The rationale behind this is that equivalent plastic strain is more related to plasticity than equivalent total strain. However, DIC analysis does not allow to separate the elastic and plastic components of strain, resulting in the necessity to use total strain output. Slip lines are obtained by analysis of strain output along a fine grid of points.

### 3 RESULTS AND DISCUSSION

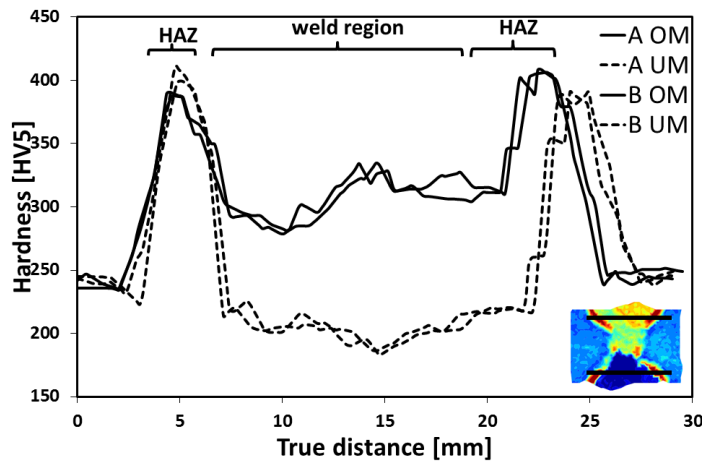
#### 3.1 Experimental results

##### 3.1.1 Hardness mapping

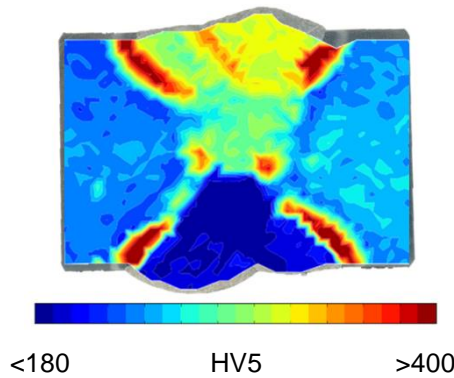
Obtained contour plots of hardness maps are given in Figure 3a and Figure 3b. Both contour plots are created using specimens (A and B) which are separated 165 mm from each other in longitudinal direction of the welded connection.



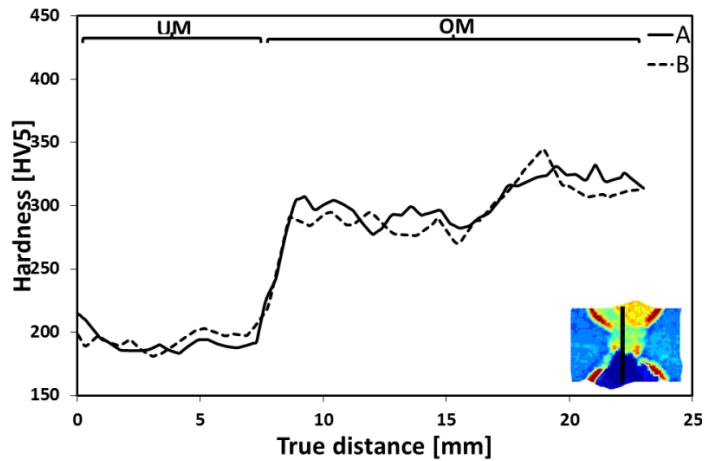
(a)



(c)



(b)



(d)

Figure 3: Hardness maps and traverses

Two horizontal traverses are taken close to the surface (approximately 2.5 mm below the plate surface), one through the under-matching region (UM) and one through the over-matching region (OM) (Figure 3c). For a hardness traverse taken in the vertical direction (a root-to-cap traverse), a hardness jump of roughly 100 HV is observed at the UM/OM interface. The similarity between both hardness maps is notable and therefore further investigation is based on the one shown on Figure 3a.

The remainder of this section is a discussion on the results which are obtained from the SENT tests. Four tests have been performed, two OM (specimens OM-1 and OM-2) and two UM (specimens UM-1 and UM-2) are discussed in this article. A closer look is taken at the analysis of the DIC images which are taken during the test.

### 3.1.2 Specimens with notch in OM region

Figure 4 presents the DIC images of specimens OM-1 and OM-2. Top figures show the equivalent strain  $\epsilon_1$  at yielding ( $P_y$ , defined using the twice elastic slope method [16]) and bottom figures show  $\epsilon_1$  at maximum load ( $P_{\max}=1.11P_y$  for OM-1,  $P_{\max}=1.17P_y$  for OM-2). Recognisable on the bottom figures of both specimens are zones where the equivalent strain is highest. From these images, the slip lines are found using the procedure which is briefly introduced in section 2.3.2. As the initial images of the test do not show clear paths of maximum equivalent strain, the slip line analysis does only show proper results starting from a certain point during the test. For OM-1, the first clear slip line is recorded while  $P=180.59\text{kN}$  ( $=0.89P_{\max}$  or  $0.98P_y$ ) and for OM-2 at  $P=138.93\text{kN}$  ( $=0.67P_{\max}$  or  $0.78P_y$ ).

Several observations are made with regards to the propagation of the slip lines during the test. Firstly, it is noticed that the slip lines translate toward each other as the test continues. This is intuitively normal, as when the crack propagates, this crack growth is translated into the translation of the slip lines vertically. Secondly, the slip lines tend to bend inwards (closer to the mid plane) as the distance to the surface becomes smaller. This can be explained by the bending of the specimen. As the crack propagates, a bending moment is imposed due to the misalignment of the applied force and the centre of the remaining ligament. This causes the stress state to change slightly, which influences the slip lines.

The slip lines compared to their position on top of the hardness map in un-deformed position allows for interpretation of their evolution with respect to the heterogeneity of the weld. Figure 5 and Figure 6 show the hardness map as discussed in section 3.1.1, where the dotted black lines indicate the edges of the specimens and the vertical black line the notch. The white lines represent the slip lines at the point of maximum force. From the figures, it is clear that the slip lines attempt to find their way through the zones of lower hardness and properties. This confirms the intuitively obvious path of least resistance.

Figure 10 shows the slip line angle (defined as the angle with respect to longitudinal direction, see Figure 5; average value over the left and right slip line path) as a function of the CTOD at that moment during the test. The value presented is the average angle of the entire slip line. Keeping the effect of unclear initial images in mind, the angles show a constant value, with a slight negative trend. For both specimens, the average slip line angle of the right slip line for OM-1 ( $47^\circ$ ) and the average slip line angle on the left of the notch for OM-2 ( $51^\circ$ ) are higher than the theoretically  $45^\circ$  observed in base metal. The left average angle for OM-1 ( $43^\circ$ ) and the right average angle of OM-2 ( $44^\circ$ ) are closer to the theoretical  $45^\circ$ .

### 3.1.3 Specimens with notch in UM region

Similar to specimens OM-1 and OM-2, Figure 7 shows the DIC images of specimens UM-1 and UM-2. Top figures show the equivalent strain at yielding and bottom at maximum load ( $P_{\max}=1.31P_y$  for UM-1,  $P_{\max}=1.18P_y$  for UM-2). The figures are here positioned in accordance to the previous figures in the article, OM side upward, UM side downward.

Figure 8 and Figure 9 show the slip line at maximum force (white line) and both are plotted on the hardness map of the specimen in the un-deformed position. Similar conclusions as with specimens OM-1 and OM-2 can be drawn here with respect to the slip lines' tendency to avoid regions of high hardness. Also, for both specimens, there is a sudden change in direction of the right slip line during the test around 97% of the maximum force. This phenomenon is attributed to the assumed definition of the slip lines. They are defined as the path of maximal equivalent strain.

Figure 11 shows the slip line angles in a similar way as for specimens OM-1 and OM-2. Slip lines in the UM regions emerged when the crack driving force (CTOD) was higher than OM-1 and OM-2. Once there, the lines remained constant in angle, except for the right slip line of UM-1, which is due to the sudden change in direction as mentioned above. There is a difference in global average right slip line angle between the specimens. The right slip line results in  $47^\circ$  for UM-1 and  $44^\circ$  for UM-2. The left slip line results are equal ( $51^\circ$  for UM-1 and  $51^\circ$  for UM-2).

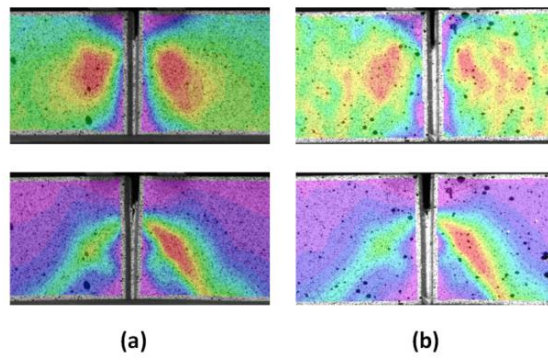


Figure 4: Strain patterns of specimens with notch in OM region (a) OM-1, (b) OM-1

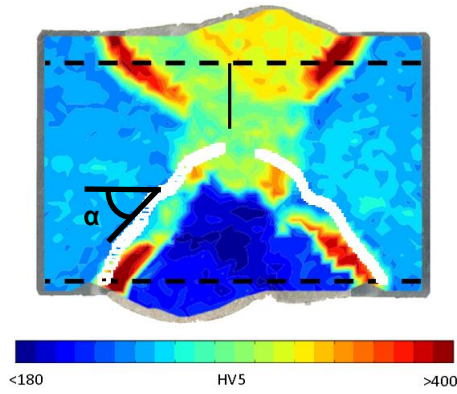


Figure 5: Slip lines at maximum force (OM-1)

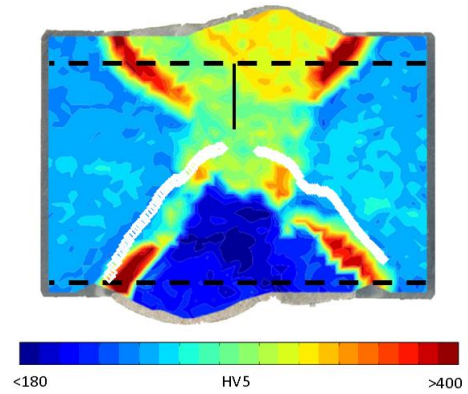


Figure 6: Slip lines at maximum force (OM-2)

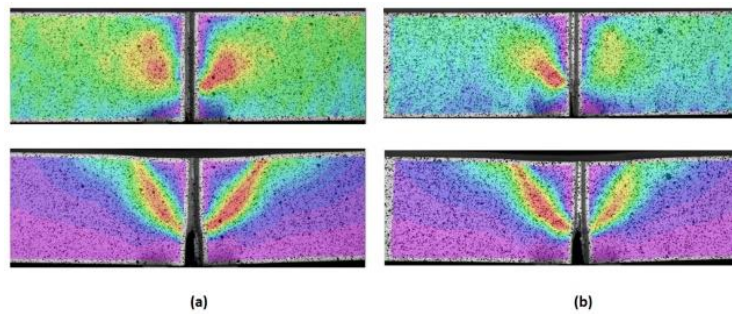


Figure 7: Strain patterns of specimens with notch in UM region (a) UM-1, (b) UM-2

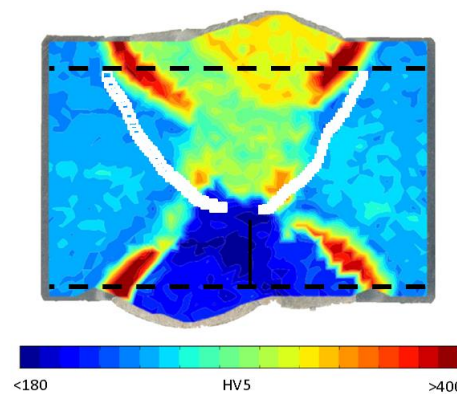


Figure 8: Slip lines at maximum force (UM-1)

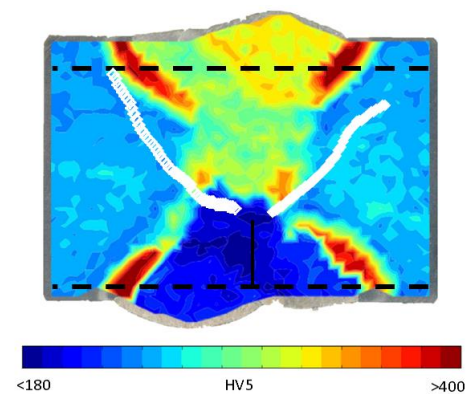


Figure 9: Slip lines at maximum force (UM-2)

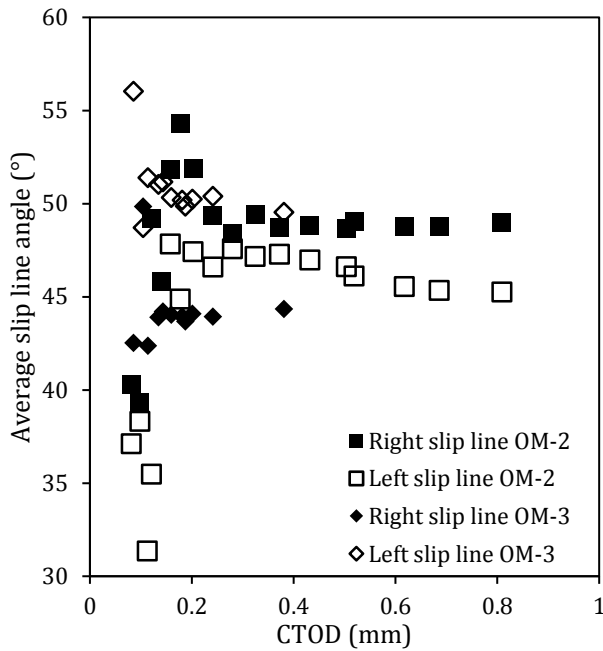


Figure 10: Slip line angles in function of the CTOD for the OM specimens

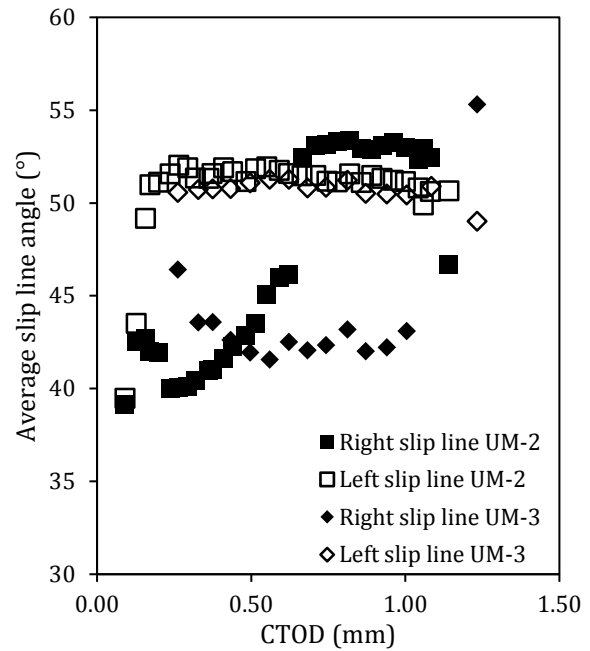


Figure 11: Slip line angles in function of the CTOD for the UM specimens

### 3.2 Numerical results

#### 3.2.1 Slip line analysis

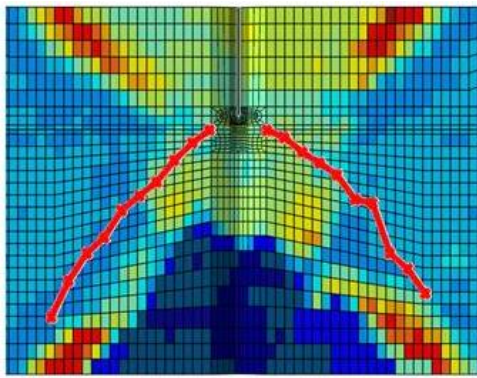
Two simulations have been performed with the in-house ABAQUS® model described in section 2.3.1. One specimen has its notch located in the OM region, whereas the other one has its notch in the UM region. The obtained slip lines are placed on top of the hardness map, to interpret and analyse the path followed by the slip lines in the heterogeneous connection. The visualised slip lines are the ones at the end of the test where  $P=P_{max}$ . Consider first the simulation where the notch is in the OM region. Figure 12 (a) represents the slip line on top of its hardness map where the original crack depth is indicated as a black line. The slip lines start, at each side of the notch, from the side groove and evolve with a linear trend towards the specimen's surface. The slip lines follow the path of least resistance. This can be seen as they tend to find regions of low hardness. The corresponding slip line angles are plotted in Figure 12 (b). The angles of the left slip line evolve from 45° to an average 49°, which is relatively higher than the theoretical 45° obtained in base material. For the right slip line, slightly higher angles are observed. There the angles evolve from 45° towards an average of 51°.

For the second simulation, the notch is located in the UM region. As visualised in Figure 13 (a) similar observations are made as for the specimen having a notch in the OM region. The slip lines have a linear trend and follow the path with the lowest material properties. However, higher slip line angles are observed as shown in Figure 13 (b). For the slip line on the right of the notch, an average slip line angle of 50° is found. The angles of the slip lines on the left side have an average value of 52°.

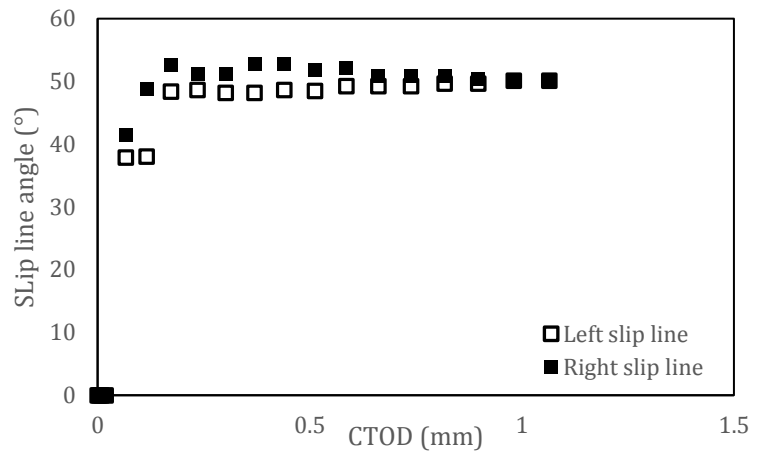
Comparing the results of both OM and UM, it is found that larger slip line angles are obtained when the notch is in the UM region. However, in both cases the slip lines show a relatively linear trend and the slip line angles at one side of the notch are higher compared to the ones at the other side.

### 3.3 Comparison and discussion

Comparing the results of the experiments with the simulations leads to the validations of the numerical model. In both cases, for all specimens, the slip lines avoid the harder regions within the weld by following the path of least resistance. For the specimens with the notch in the OM region, the experiments and simulations show higher slip line angles for the left slip line than for the right slip line. However, the slip line angles of the left slip line obtained from the simulations (around 50°) are slightly larger than from the experiments (43° for OM-1, 44° for OM-2). Similar observations are made for the specimens with a notch in the UM region. The evolution of the angles is a consequence of the path followed by the slip lines. As the slip lines tend to avoid the harder regions, the slip line angles reflect these deviations.

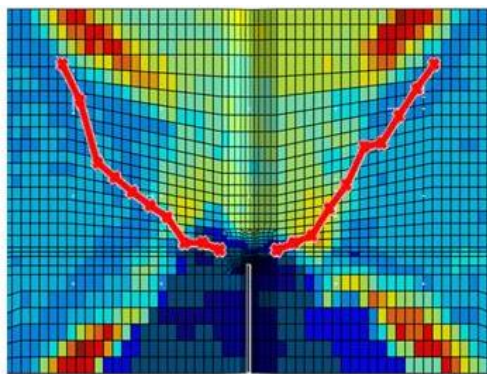


(a)

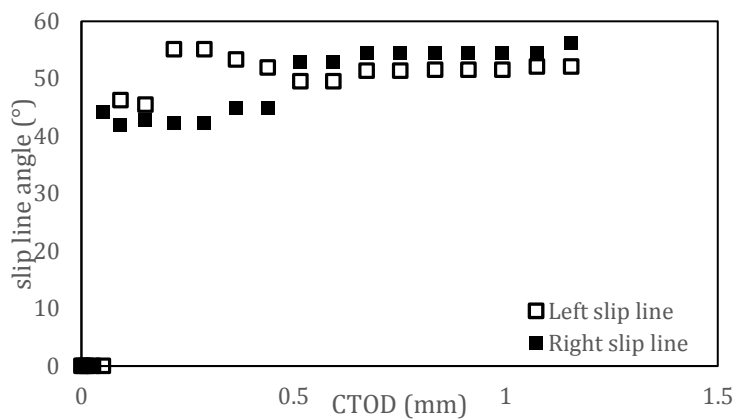


(b)

Figure 12: Results simulations notch in OM region (a) Slip lines, (b) Slip line angles



(a)



(b)

Figure 13: Results simulations notch in UM region (a) Slip lines, (b) Slip line angles

#### 4 CONCLUSION

The study at hand investigates the effect of heterogeneity within the weld material. Both SENT experiments as well as simulations with a model have been performed. It can be concluded that slip line appearances of the experiments and simulations agree, in the sense that regions of high hardness are avoided. Slip line angles obtained by linear regression reflect the changes in slip line direction as the test proceeds (characterised by a growing CTOD and crack propagation).

#### 5 ACKNOWLEDGEMENTS

The authors would like to acknowledge the FWO Vlaanderen (grant nr. G0609.15N), and the University of Maribor for the production and delivery of the test material.

#### 6 REFERENCES

- [1] K.-H. Schwalbe and M. Koçak, "Mis-Matching of Welds," *ESIS: Mechanical Engineering Publications*, vol. 17, 1994.
- [2] K.-H. Schwalbe and M. Koçak, "Second International Symposium on Mis-Matching of Interfaces and Welds," 1997.
- [3] *BS7910(2005): Guide to methods for assessing the acceptability of flaws in metallic structures*, 2005.

- [4] *ASTM E384-11 - Standard Test Method for Knoop and Vickers Hardness of Material*, 2012.
- [5] S. Hertelé, W. De Waele, M. Verstraete, R. Denys and N. O'Dowd, "J-integral analysis of heterogeneous mismatched girth welds in clamped single-edge notched tension specimens," *International Journal of Pressure Vessels and Piping*, pp. 95-107, 2014.
- [6] M. A. Verstraete, R. M. Denys, K. Van Minnebruggen, S. Hertelé and W. De Waele, "Determination of CTOD resistance curves in side-grooved Single-Edge Notched Tensile specimens using full field deformation measurements," *Engineering Fracture Mechanics*, pp. 110:12-22, 2013.
- [7] M. Verstraete, S. Hertelé, W. De Waele, R. Denys and K. Van Minnebruggen, "Measurement of Ductile Crack Extension in Single Edge Notch Tensile Specimens," *15th International Conference on Experimental Mechanics*, 2012.
- [8] E. Fagerholt, E. Østby, T. Børvik and O. S. Hopperstad, "Investigation of failure in small-scale SENT test of a welded X80 pipeline steel using Digital Image Correlation with node splitting," *Engineering Fracture Mechanics*, vol. 96, pp. 276-293, 2012.
- [9] M. A. Verstraete, W. De Waele, K. Van Minnebruggen and S. Hertelé, "Single-specimen evaluation of tearing resistance in SENT testing," *Engineering Fracture Mechanics*, vol. 148, pp. 324-336, 2015.
- [10] *BS8571(2014): Method of test for determination of fracture toughness in metallic materials using single edge notched tension (SENT) specimens*, 2014.
- [11] S. Hertelé, N. O'Dowd, K. Van Minnebruggen, M. Verstraete and W. De Waele, "Fracture mechanics analysis of heterogeneous welds: Numerical case studies involving experimental heterogeneity patterns," *Engineering Failure Analysis*, vol. 58, pp. 336-350, 2015.
- [12] M. A. Verstraete, S. Hertelé, R. M. Denys, K. Van Minnebruggen and W. De Waele, "Evaluation and interpretation of ductile crack extension in SENT specimen using unloading compliance technique," *Engineering Fracture Mechanics*, vol. 115, pp. 190-203, 2014.
- [13] G. Shen, J. A. Gianetto and W. R. Tyson, "Measurement of J-R curves using single specimen technique on clamped SE(T) specimens," Osaka, 2009.
- [14] S. Naib, K. Van Minnebruggen, W. De Waele and S. Hertelé, "Sensitivity study of crack driving force predictions in heterogeneous welds using Vickers hardness maps," 2016.
- [15] F. Van Gerven, "Slip line analysis of heterogeneous flawed welds loaded in tension," 2014-2015.
- [16] *ASME: BPVC Section III-Rules for Construction of Nuclear Facility Components-Division 1-Subsection NF-Supports*, 2017.